

**30-Year Atmospheric Temperatures Derived from Satellite  
Microwave Sounding Instruments Using a 1D-Var Approach**

Fuzhong Weng<sup>1</sup>, Kunghwa Wang<sup>2</sup>, and Xiaolei Zou<sup>3</sup>

1. National Environmental Satellite, Data & Information Service, National  
Oceanic and Atmospheric Administration

2. Earth System Science Interdisciplinary Center (ESSIC)  
University of Maryland

and

3. Department of Earth, Ocean and Atmospheric Sciences, Florida State  
University

Submitted to

*J. of Climate.*

<sup>1</sup>Corresponding author address: Dr. Fuzhong Weng, NOAA/NESDIS, Room 712, 5200 Auth Road,  
Camp Springs, MD 20746, Email: Fuzhong.Weng@noaa.gov

April , 2012

## **Abstract**

In past 30 years, satellite observations of the microwave radiation emitted from the atmosphere have been utilized for deriving the atmospheric temperature profiles. Specifically, the radiance measurements from Microwave Sounding Unit (MSU) on board the early National Oceanic and Atmospheric Administration (NOAA)-6 to NOAA-14 and Advanced Microwave Sounding Unit-A (AMSU-A) on board NOAA-15 to -19 have been reprocessed to form a fundamental climate data record (FCDR). The FCDR were inter-calibrated and the major anomalies related to the instrument calibration were removed. In this study, a climatology temperature profile is used as an initial guess in one-dimensional variation (1D-Var) retrieval to further derive the thematic CDR (TCDR) of atmospheric temperatures that are appropriate for climate change study. The retrieval temperature profiles are collocated with Global Positioning System (GPS) radio occultation (RO) data over global oceans and compared with the GPSRO temperature profiles. It is shown that the assimilation of MSU/AMSU-A four channels into the climatology profiles can produce a reasonably accurate temperature analysis in the troposphere, and the assimilation of AMSU-A 15 channels available since 1998 allows such a TCDR to be extended to the stratosphere and higher. The global climate trend of the atmospheric temperature deduced from the TCDR not only confirms a warming in the troposphere and a cooling in the stratosphere, but also a stronger warming in the upper troposphere than in the low troposphere.

## 1. Introduction

The Microwave Sounding Unit (MSU) and the Advanced Microwave Sounding Unit (AMSU) on board the National Oceanic and Atmospheric Administration (NOAA) polar-orbiting satellites measure the upwelling microwave radiation emitted primarily from atmospheric oxygen. Since the oxygen concentration is nearly uniformly distributed through atmosphere and is stable with time, MSU and AMSU are unique satellite instruments for remotely sounding the atmospheric temperature and for climate research. The MSU instruments on board NOAA-6 to NOAA-14 have four channels and provided data from 1979 to 2006. The MSU channel characteristics are provided in Table 1. Each of the four channels provides measurements of a weighted average of radiation emitted from a particular layer of the atmosphere at a specified frequency. The relative contributions to the total measured radiance from different levels of the atmosphere are quantified by the so-called weighting function (WF), which is channel-dependent (Fig. 1). The measured radiation is most sensitive to the atmospheric temperature at the altitude where WF reaches the maximum value. The AMSU instruments on board NOAA-15 to NOAA-19 have 15 channels (see Table 2), in which four channels (i.e., AMSU-A channels 3, 5, 7, and 9) are similar, but not identical, to the four MSU channels in frequency. The other 11 AMSU channels sample more atmospheric layers than MSU. For convenience, AMSU channels 3, 5, 7 and 9 are to be referred to as MSU-like AMSU channels hereafter. By putting together MSU and the MSU-like AMSU channels, a long-term series of global satellite microwave

sounding data of more than 30 years is available for climate study related to atmospheric temperature changes.

In history, all MSU and AMSU instruments from NOAA-6 to NOAA-19 were designed for day-to-day operational uses in weather forecasting. The requirements on satellite data calibration for climate studies are different from weather forecasting applications. Issues such as variable calibration accuracy (or bias) associated with each satellite instrument, and accuracy (bias) changes with respect to time due to the satellite orbital drift must be resolved since they may be mistakenly interpreted as climate influences. Currently, three fundamental climate data records (FCDRs) were established, in which MSU and AMSU measurements were carefully inter-calibrated and non-climate influences were mostly removed. These three FCDRs were deduced from the same MSU/AMSU brightness temperature measurements by three different research groups: the University of Alabama at Huntsville (UAH) (Christy et al., 1998, 2000, 2003), the Remote Sensing Systems (RSS) (Mears et al. 2003, Mears and Wentz 2009), and NOAA/Center for Satellite Applications and Research (STAR) (Zou et al., 2006, Vinnicov and Grody, 2007, Zhou et al., 2009, 2010). Major differences among three FCDRs come from different data adjustments that are made for instrument calibration and diurnal corrections.

Pioneer investigations on climate change using MSU channel 2 and AMSU channel 5 brightness temperature measurements from the above-mentioned UAH FCDR showed a small warming trend in the mid-troposphere (referred to as  $TB_2$  trend hereafter) (Spencer and Christy, 1992a, b; Christy et al. 1998, 2000, 2003).

However, the T2 warming trends derived from the RSS FCDR (Mears et al. 2003, Mears and Wentz 2009) and the NOAA STAR FCDR (Zou et al., 2006, 2009, 2010) were much larger than that from the UAH FCDR. The differences in the  $TB_2$  trends from the three FCDRs exceed the widely accepted accuracy requirement of 0.01-0.02 K/decade for the climate trends (Ohring et al., 2004). Further investigations on structural differences and/or similarities among these different studies in constructing their respective brightness temperature time series are required for understanding the resulting trend differences.

The fact that the brightness temperature for each MSU or AMSU channel represents a weighted temperature average within an atmosphere layer averaged by the WF introduces many complications to the interpretation of the warming trends deduced from satellite brightness temperatures. For examples, MSU channel 2 ( $TB_2$ ), which has a quite broad WF with its maximum located at 350 hPa and the half-power located at about 40 hPa, only broadly represents the troposphere. It also includes a significant contribution from the lower stratosphere. In order to remove the stratospheric influence, Spencer et al. (1992) attempted to generate a synthetic “low-middle-tropospheric” channel,  $TB_{2LT}$ , by subtracting signals at different view angles of MSU channel 2. The resulting “ $TB_{2LT}$  channel” has its WF maximum located at about 650 hPa. While stratospheric influences are removed in  $TB_{2LT}$ , other complications such as noise amplifications and surface emissivity influences are introduced (Hurrell and Trenberth, 1998). Fu et al. (2004) proposed a different approach for removing the stratospheric contribution in  $TB_2$ . Instead of combining

the data from a single MSU channel 2 ( $TB_2$ ) at different viewing angles, Fu et al. (2004) generated a synthetic free-tropospheric channel “ $TB_{850-300}$ ” by combining data from two MSU channels (i.e., channels 2 and 4) at the same FOVs. Specifically,  $TB_{850-300}$  is defined as follows:  $TB_{850-300} = a_2TB_2 + a_4TB_4$ , where  $a_2 = 1.156$  and  $a_4 = 20.153$ . The values of  $a_2$  and  $a_4$  were obtained by a least-squares regression of radiosonde-simulated <sup>1</sup>  $a_2TB_2 + a_4TB_4$  to vertically integrated radiosonde temperatures from 850 hPa to 300 hPa. A warming trend of 0.09 K/decade and 0.18 K/decade for the period from 1979 to 2001 was obtained based on the UAH  $TB_{850-300}$  and the RSS  $TB_{850-300}$  data, respectively. The trend values of  $TB_{850-300}$  are much larger than the trend values of  $TB_2$ , which is 0.01 K/decade and 0.1 K/decade based on the UAH and RSS FCDRs, respectively. Limitations in using  $TB_{850-300}$  for climate study arise from the fact that radiosondes and radiative transfer model (RTM) simulated brightness temperatures were used for generating the weighting coefficients ( $a_2$  and  $a_4$ ) for channels 2 and 4. Radiosondes are limited in its spatial coverage over land, very few over oceans, and subject to a host of complications, including changing instrument types, artificial shifts, radiative warming of radiosonde instruments by sunlight, and lack of metadata. It is also reminded that neither  $TB_{2LT}$  nor  $TB_{850-300}$  methods had made a full use of all four available MSU channels for investigating global warming trends.

This study aims at directly deriving the atmospheric temperature at different

---

<sup>1</sup> A total of 87 stations for the period 1958–97 (Lanzante et al., 2003).

pressure levels from all four MSU and MSU-like AMSU channels so that the climatology of the atmospheric temperature at specific pressure levels could be deduced globally. Specifically, the one-dimensional variational (1D-Var) Microwave Integrated Retrieval System (MIRS), which was originally designed for day-to-day numerical weather prediction (NWP) applications (Liu and Weng, 2005; Boukabara et al., 2011), is modified and a preliminary global climate data record (CDR) of atmospheric temperature is deduced. Section 2 will briefly discuss the MSU and AMSU instrumentation and provide an overview of the existing datasets used for this study. Key components of the MIRS for deriving an atmospheric temperature CDR dataset from MSU and AMSU satellite brightness temperature observations are described in Section 3. A detailed analysis of the 1D-Var MIRS results is presented in Section 4. Verifications of the 1D-Var derived temperature profiles with GPS radio occultation (RO) data are provided in Section 5, along with a discussion on the 30-year averaged global temperature distributions at different pressure levels deduced from MSU and AMSU data. The paper concludes in Section 6.

## **2. MSU/AMSU Brightness Temperature Datasets**

### **2.1 A Brief Description of MSU and AMSU Characteristics**

The first MSU was launched on board the first NOAA satellite Tires-N in 1978 and made the measurements at four frequencies (50.3, 53.74, 54.96 and 57.95 GHz). The channels 1 and 3 measure the radiance of the vertical polarization at nadir whereas channels 2 and 4 correspond to that of the horizontal polarization. The MSU antenna system requires to have a nominal beam width of  $7.5^\circ$  at the half-power

points which corresponds to an along scan resolution of 105 km near nadir. The MSU scans across the track within  $\pm 47.4^\circ$  from the nadir and produces a scan swath of 2400 km. Beam positions 1 and 11 are the extreme scan positions of the Earth views, each separated by  $9.47^\circ$  while beam position 6 is at the nadir direction. The radiation from the nadir position arises from the atmosphere in the vertical direction, which is ideal for weather and climate applications. Onboard calibration using blackbody and cold space observations is performed once every 25.6 seconds for each scan line. The main MSU characteristics are provided in Table 1.

The AMSU has been operational since 1998 and is flown onboard NOAA-15 to 19 and Metop-A satellites. Similar to MSU, AMSU is mainly designed to vertically probe the atmosphere in nearly all-weather condition (except for heavy precipitation). It contains 15 channels quantifying the thermal radiation at microwave frequencies ranging from 23.8 to 89.0 GHz (see Table 2). The AMSU-A has an instantaneous field-of-view of  $3.3^\circ$  and scans  $\pm 48.7^\circ$  from nadir with 15 different viewing angles at both sides. Atmospheric temperature profiles are primarily based on the measurements obtained at channels near 50-60 GHz. In particular, the AMSU-A sounding channels (3-14) respond to the thermal radiation at various altitudes, whereas channels 1 and 2 are primarily designed for obtaining the information on surface and cloud properties. Since the satellite provides a nominal spatial resolution of 48 km at its nadir, the temperature perturbations from synoptic scale to large mesoscale can be depicted reasonably well.

Figure 1 displays the WFs for four MSU and MSU-like AMSU channels at a  $0^\circ$  local zenith angle. The MSU channel 2 has two bands located at both sides of the center frequency and AMSU channel 5 has only one band. The center frequency absorption is covered in AMSU channel 5, but not in MSU channel 2. Such a

difference is reflected in the WFs shown in Fig. 1. The WF of the MSU channel 4 is slightly broader and peaks slightly higher than the AMSU-A channel 9 due to slight differences in center frequency and bandwidth for these two corresponding channels. Similar but smaller differences exist between MSU channel 3 and AMSU channel 7. The WF differences between MSU channel 1 and AMSU channel 3 are smallest.

## **2.2 The NOAA/STAR MSU/AMSU Dataset**

Merging multi-year satellite data from different MSU instruments requires careful adjustments of the observations to account for drifts caused by orbital decay and changes in local observing time, and determination of inter-satellite offsets and errors caused by changes in the temperature of the calibration sources. NOAA/STAR has recently released its level-1c inter-calibrated 30+year (1979-2011) MSU/AMSU observations (Zou et al., 2011). The instrument non-linearity is updated using simultaneous nadir overpassing (SNO) data. Diurnal-drift errors, incident angle errors, warm target temperature correction, and residual inter-satellite biases are accounted for. This dataset is used as input for the 1D-Var temperature retrieval of this study. Figure 2 provides MSU data periods onboard NOAA's earlier eight polar-orbiting satellites (from NOAA-6 to NOAA-14) and the AMSU-A data period on NOAA-15, which are used in this study.

It is worth mentioning that there are two other MSU/AMSU datasets that are also available for community uses. RSS has recently developed version 3.3 Level-1c inter-calibrated 30+year (1979-2011) MSU observations and includes the data from the AMSU instruments onboard NOAA-15, AQUA, NOAA-18, and MetOp-A. UAH has generated version 5.2 level-1c inter-calibrated 25+year (1979-2004) MSU observations with nonlinearity correction applied to each instrument. Diurnal-drift errors, incident angle errors and residual inter-satellite biases are accounted for in

these products. A detailed inter-comparison among the above-mentioned three datasets is being carried out and their potential impacts on temperature retrievals will be assessed in subsequent studies.

### 3. The 1D-Var Approach

#### 3.1 Formulation

The 1D-Var satellite data retrieval algorithm searches for a minimum solution  $\mathbf{x}^*$  to the following cost function

$$J(\mathbf{x}) = \frac{1}{2}(\mathbf{x} - \mathbf{x}_b)^T \mathbf{B}^{-1}(\mathbf{x} - \mathbf{x}_b) + \frac{1}{2}(\mathbf{H}(\mathbf{x}) - \mathbf{y}^{obs}) \mathbf{R}^{-1}(\mathbf{H}(\mathbf{x}) - \mathbf{y}^{obs}) \quad (1)$$

i. e.,

$$J(\mathbf{x}^*) \leq J(\mathbf{x}) \quad \forall \mathbf{x} \text{ in the neighborhood of } \mathbf{x}_b. \quad (2)$$

In (1),  $\mathbf{x}$  is the control variable vector,  $\mathbf{x}_b$  is the background state variable vector;  $\mathbf{B}$  is the background error covariance matrix;  $\mathbf{y}$  includes brightness temperature observations from MSU or MSU-like AMSU channels;  $\mathbf{H}(\mathbf{x})$  represents the forward operator such as Community Radiative Transfer Model (CRTM) which calculates the radiance at the top of the atmosphere for a given set of input parameters including the atmospheric state variables  $\mathbf{x}$ ;  $\mathbf{R}$  is the sum of observation error covariance matrix ( $\mathbf{O}$ ) and CRTM error covariance matrix ( $\mathbf{F}$ ). The matrices  $\mathbf{H}$  and  $\mathbf{H}^T$  are the tangent linear operator and adjoint operator of the CRTM operator  $H$ , respectively. The state variable ( $\mathbf{x}$ ) in (1) includes the atmospheric temperature profile, water vapor profile, and surface parameters (e.g., sea surface temperature, surface emissivity). A climatology profile is taken as the background field ( $\mathbf{x}_b$ ).

The minimum solution  $\mathbf{x}^*$  in (2) is obtained through an iterative procedure (Zou

et al., 1993):

$$\mathbf{x}^{(k+1)} = \mathbf{x}^{(k)} + \alpha_k \mathbf{d}^k \quad (3)$$

where  $k$  ( $k=1, 2, \dots$ ) is the iteration number,  $\mathbf{d}^k$  is the search direction at the  $k^{\text{th}}$  iteration and is constructed from the gradient vectors of current ( $\mathbf{g}_k$ ) and previous ( $\mathbf{g}_{k-1}, \dots, \mathbf{g}_0$ ) iterations, where

$$\mathbf{g}_k \equiv \nabla J|_{\mathbf{x}^{(k)}} = \mathbf{B}^{-1}(\mathbf{x}^{(k)} - \mathbf{x}_b) + \mathbf{H}^T \mathbf{R}^{-1}(H(\mathbf{x}^{(k)}) - \mathbf{y}^{obs}) \quad (4)$$

and  $\alpha_k$  is the step size at the  $k^{\text{th}}$  iteration and satisfies

$$J(\alpha_k) \equiv J(\mathbf{x}^{(k)} + \alpha_k \mathbf{d}_k) \leq J(\mathbf{x}^{(k)} + \alpha \mathbf{d}_k) \quad \forall \alpha \in [0,1] \quad (5)$$

The above minimization process (1)-(5) is carried out in two sequences, one assuming a clear-sky condition for CRTM simulation and the other cloudy conditions. The largest iteration numbers in the two sequences are set to two and seven, respectively. The minimization procedure is stopped if

$$\varepsilon \equiv \sum_{ich=1}^4 \frac{(y_{ich}^{obs} - y^{(k)})^2}{(NE\Delta T_{ich})^2} < 1 \quad (6)$$

The value of  $\mathbf{x}^{(k)}$  satisfying the above convergence criteria is taken as  $\mathbf{x}^*$  (e. g., the final 1D-Var retrieval product). In other words, the final 1D-Var solution ( $\mathbf{x}^*$ ) represents an atmospheric state from which the CRTM-simulated brightness temperatures compare favorably with satellite measurements.

A schematic illustration of the 1D-Var is shown in Fig. 3. More details of the 1D-Var can be found in Liu and Weng (2002) and Boukabara et al., (2011).

### 3.2 Twin Experiments

A total of four twin experiments is firstly carried out to examine the sensitivity of 1D-Var temperature retrievals to water vapor and sea-surface temperature (SST)

variables. Using twin experiments to assess the impacts of SST and water vapor on temperature retrievals are convenient since the truth atmospheric profiles are known. The National Centers for Environmental Prediction (NCEP) Global Forecast System (GFS) 6-h model forecasts is taken as the “true” atmosphere for generating simulated brightness temperature “observations”. The NCEP GFS forecast fields are available at a horizontal resolution of  $1^\circ \times 1^\circ$ , and a temporal resolution of six hours. There are 26 vertical layers which are unevenly spaced from 1000 hPa to 10 hPa. This dataset is available publicly in real time since 1999, enabling researchers to initialize data assimilation cycles and numerical weather prediction models as well as for satellite data evaluations.

The cost function that is minimized in twin experiments is the same as (1) except for the observations  $\mathbf{y}^{obs}$ , which are replaced by the synthetic observations  $\mathbf{y}^{“synthetic obs”}$ . This synthetic AMSU observations are obtained by the following two steps: (i) the global observations of AMSU channels 3, 5, 7 and 9 on January 24, 2011 are firstly simulated by CRTM using realistic satellite scan geometry and geo-location information and the NCEP GFS 6-h forecasts as input; and (ii) random errors with the AMSU “NEDT” values listed in Table 2 are then added to the brightness temperature simulations. The four twin experiments only differ in the selection of the control variable  $\mathbf{x}$ . In the first experiment (EXP1),  $\mathbf{x}$  includes temperature, water vapor and sea-surface temperature (SST). The second experiment (EXP2) is the same as EXP1 except that SST is fixed. The third experiment (EXP3) is the same as EXP1 except that water vapor is fixed. In the fourth experiment (EXP4), both SST and water vapor

are fixed.

Figure 4 presents the global root-mean-square error (rmse,  $\sigma_A$ ) and the difference of rmse between the analysis and the first guess ( $\sigma_A - \sigma_G$ ) of temperature retrievals from these four experiments compared with the truth. As shown in Fig. 4, an inclusion of water vapor and SST in the state control variable can improve the temperature retrievals throughout the atmosphere. Fixing SST has a negligible impact on the temperature retrieval, especially below 400 hPa. It is therefore determined that both water vapor and SST will be included in the 1D-Var real-data experiments conducted in this study.

### 3.3 Sensitivity of MSU Brightness Temperatures to Cloud and Water Vapor

Although MSU and AMSU are designed mainly for sounding the atmospheric temperature in all weather conditions, they are also sensitive to cloud and water vapor which are highly variable in the atmosphere. Figure 5 displays the differences of CRTM-simulated brightness temperatures with ( $T_b^{clear-sky}$ ) and without ( $T_b^{cloud}$ ) neglecting the scattering and emission effects of clouds in the radiative transfer process under cloudy conditions. Each data point in Fig. 5 corresponds to a  $1^\circ \times 1^\circ$  grid (i.e., the NCEP GFS 6-h model forecast resolution). The cloud liquid water mixing ratio profiles from NCEP GFS 6-h model forecasts are vertically integrated to derive the total column cloud liquid water path (LWP). At each model grid, the cloudy radiance simulation is firstly performed with all input variables from NCEP GFS 6-h forecast fields, which will be denoted as  $T_b^{cloud}$ , and then the same radiance simulation is carried out except for setting LWP to zero to obtain cloudy radiance

simulation, which is denoted  $T_b^{clear-sky}$ . Differences between these two simulations,  $T_b^{cloud} - T_b^{clear-sky}$ , reflect the cloud effects on brightness temperature biases. In this assessment, simulations over oceanic grids are used since the impacts from clouds on brightness temperature are much more pronounced than over land.

At AMSU channel 3, the cloud effects on brightness temperature increase the brightness temperature ( $T_b^{cloud} \geq T_b^{clear-sky}$ ). The larger the cloud LWP is, the greater the cloudy radiance  $T_b^{cloud}$  is (see Fig. 5a). Note that the AMSU channel 3 has a central frequency located at 50.30 GHz, which is away from the center of the oxygen absorption band. Under clear-sky atmospheric conditions, brightness temperature is much lower than the physical ocean surface temperature ( $T_s$ ) due to small surface emissivity over ocean (i.e.,  $\varepsilon \approx 0.5$ ). When cloud is present in the atmosphere, it emits more radiation than surface radiation due to an equivalent higher emissivity of cloud. The biases introduced by cloud effects could be more than 10 K. For AMSU channel 5, which has a weighting function that peaks at 650 hPa, the cloud effects reduce the brightness temperature, i. e.,  $T_b^{cloud} - T_b^{clear-sky} \leq 0$ . The magnitude of the negative impact of cloud on brightness temperature tends to increase as the cloud LWP increases. For a cloud above the peak of AMSU channel 5, the radiation emitted from the cloud layer is less than that from the clear-sky atmosphere since the cloud-layer temperature is lower than the atmospheric temperature near the peak of AMSU channel 5 (i.e., 650 hPa). The brightness temperature biases for this channel could be as large as 5-6 K. Since the majority of clouds in the atmosphere are below 250 hPa, the impacts of clouds on brightness temperatures at AMSU channel 7 are

rather small and the biases are typically less than 2 K (Fig. 5c). The impacts of clouds on AMSU channel 9 are generally negligible (Fig. 5d). Since the impacts of clouds on AMSU channels 3 and 5 are very significant, the state variable in the 1D-Var must consider the cloud liquid water content profiles. Alternatively, the measurements under cloudy conditions should be detected and excluded. The later is chosen for this study and more details can be found in Section 4.

With the same token, the impacts of atmospheric water vapor on AMSU temperature sounding channels can similarly be investigated. Figure 6 presents brightness temperature differences resulting from radiative transfer simulations with and without water vapor absorption. It is clearly demonstrated that brightness temperature of AMSU channel 3 at 50.30 GHz is strongly affected by water vapor emission (Fig. 6a). The retrieval process should include the water vapor profile in the state variable in order to obtain realistic temperature retrieval. This is consistent with the results in Fig. 4 which shows that the AMSU-like channel data assimilation results in a more accurate temperature retrieval when water vapor is included in the control state variable. Compared to AMSU channel 3, impacts of water vapor absorption for AMSU channels 5, 7 and 9 are one, two and three orders of magnitudes smaller, respectively.

## **4. Real-Data Assimilation Results**

### **4.1 Data Description**

The MSU and AMSU dataset available from June 1979 to December 2009 were assimilated for obtaining microwave temperature retrieval. From NOAA-6 to

NOAA-15, successive satellite data from second month be used to replace previous one even there are data of last satellite. NOAA-8 has only two years data and NOAA-12 missed 8 months data within 5 years period. MSU data at FOV 6 and AMSU data at FOV 15 were extracted for this study to avoid the limb bias. Monthly mean surface temperature and surface wind are available since November 1981. Assume sea surface monthly mean changes very little, surface data during 1981 and 1982 is used for MSU simulations between June 1979 and October 1981. MSU data are corrected to AMSUA channels by regression coefficient in which  $NE\Delta T$  differences between MSU and AMSU are considered.

In order to show that consistency of brightness temperature observations between MSU and AMSU-A during the over-lapping period, we show in Fig. 7 the brightness temperature correlations between NOAA-14 MSU channels and the corresponding NOAA-15 AMSU-A subset channels for SNO data in 2002, with a spatial separation being less than 100 km, and a temporal separation being less than 100 seconds. It is seen that the MSU and AMSU-A data are highly correlated, confirming a reliable bias correction for satellite observations from NOAA-14 and NOAA-15 by Zou et al. (2011).

## **4.2 Cloud Detection**

Based on the physical properties that the brightness temperatures at AMSU channel 3 (or MSU channel 1) are significantly affected by cloud liquid water and the AMSU channel 5 (or MSU channel 2) is much less sensitive to the presence of cloud liquid water, these two channels could be used for cloud detection. A cloud detection

algorithm similar to that in Weng and Grody (1993) is developed. Firstly, cloud liquid water path (LWP) is estimated from brightness temperatures at MSU channels 1 and 2 (or AMSU channels 3 and 5) using the following formula:

$$LWP = c_0 + c_1 \log(290 - T_{b,Ch1}) + c_2 \log(290 - T_{b,Ch2}) \quad (7)$$

where  $c_0 = 4.4313$ ,  $c_1 = -1.3801$  and  $c_2 = 0.4138$ . The coefficients may also depend on the range of cloud liquid water as well as scan angle.

A logarithmic form is selected in (7) due to an exponential relationship between the brightness temperature at channel 3 and cloud LWP. The coefficients  $c_1$ ,  $c_2$  and  $c_3$  in the algorithms are derived from AMSU data simulated with a set of 1900 radiosonde profiles distributed over all the geographical regions. For each profile, a cloud layer below the freezing level with a randomly selected value of liquid water content within a range of 0-0.3 g m<sup>-3</sup> is added to the profile. Since the brightness temperature over ocean is also sensitive to surface wind speed, surface wind speed is also varied within 0-10 m/s in producing the simulated dataset.

Once the coefficients  $c_1$ ,  $c_2$  and  $c_3$  in (7) is determined, the LWP can be estimated from AMSU channels 3 and 5. An LWP value greater than 0.5 g m<sup>-2</sup> indicates the presence of liquid water clouds within the satellite field of view. The cloud detection is implemented by removing all data points with estimated LWP greater than this value.

Another technique for dealing with cloud effects in the temperature retrieval is to include the cloud liquid water in the state control variable. However, a limited amount of information from four-channel MSU data on clouds makes it difficult to

simultaneously resolve all the profiles of temperature, water vapor and cloud liquid water content.

### **4.3 Numerical Results**

Figure 8 provides the mean and standard deviation of the differences between observations and model simulations before and after the 1D-Var data assimilation. Both the mean and standard deviations are reduced by more than an order of differences for channels 3, 5, 7 and 9. Before examining the 30-year variations of atmospheric temperature deduced from satellite observations, a verification of the 1D-Var results with GPS RO data is carried out first.

Accurate atmospheric temperature profiles can be derived from Global Position System (GPS) radio occultation (RO) technique. Using Constellation Observing System for Meteorology, Ionosphere and Climate/Formosa Satellite Mission #3 (COSMIC/FORMOSAT3, hereafter referred to as COSMIC for brevity) data, the atmospheric temperature profile can be as accurate as 0.05K in the middle and upper troposphere (Anthes et al., 2008). The global mean differences between COSMIC and high-quality reanalyses within the height range between 8 and 30 km are estimated to be  $\sim 0.65^{\circ}\text{C}$  (Kishore et al. 2008). In the water vapor abundant region in the lower troposphere or the ionosphere regions, GPS profiles become less accurate.

In order to also show the differences of temperature retrievals between assimilations of four subset channels and assimilations of all 15 channels, brightness temperatures of NOAA-18 AMSU-A channels during June 1-10 in 2008-2011 are assimilated. Collocation criteria between GPS ROs and NOAA-15 AMSU-A nadir

observations are set to be less than one hour in temporal differences and 50 km in spatial separations. Compared with COSMIC GPS RO data during June 1-10 in 2008-2011, the atmospheric temperature profiles from the first guess contain a negative bias in the troposphere above 950 hPa (Fig. 9a). The assimilation of AMSU-A four subset channels completely removes this mean error of the temperatures in the troposphere. A slight increase of bias is found above 250 hPa due to a rather coarse vertical resolution of the four AMSU-A subset channels in upper levels. The root-mean-square (RMS) errors of the temperature profiles are significantly reduced throughout the atmosphere by the assimilation of brightness temperatures from the AMSU-A subset channels. It is also demonstrated that assimilation of all AMSU-A channels improves the temperature retrievals in upper levels due to the added channels 10-14 above the stratosphere and above.

Figure 10 provides the monthly variations of global mean atmospheric temperatures at ten pressure levels derived from MSU/AMSU-A brightness temperatures during the 30-year periods from June 1979 to December 2009 by a 1D-Var approach. The annual variation of the atmospheric temperature is seen at all ten pressure levels. The consistency between the MSU temperature retrievals and AMSU-A temperature retrievals during the over-lapping period between NOAA-14 and NOAA-15 further confirms a successful bias correction for satellite observations from NOAA-6 to NOAA-15 based on SNO nadir-only data.

The 30-year variations of the global temperature anomaly derived from the 30-year temperature retrieval are provided in Fig. 11. It is seen that the temperature anomaly is consistently negative in the earlier years and positive in the later years below 200 hPa. A reversed sign of temperature anomaly is seen between 50-100 hPa, The vertical distribution of the global mean temperature trend and the uncertainty

calculated from the temperature retrieval from 1980-2009 is presented in Fig. 12. The decadal warming trend is about 0.5K in the low troposphere (e.g., below 500 hPa), and increases to about 0.7K around 300 hPa. A weak cooling trend is seen at 100 hPa. Trends above 50hPa are not reliable due to lack of upper-level channels.

## **5. Summary and Conclusions**

In this study, a 1D-Var method is used for detecting the global warming/cooling trends through a direct assimilation of global oceanic brightness temperatures observed by MSU and AMSU-A on board the NOAA polar-orbiting satellites over the time period from June 1978 to August 2010. A 30-year TCDR of the atmospheric temperature profiles is derived from the satellite observations for the first time. The high accuracy of the CRTM for the forward simulation of satellite observed microwave radiances makes the 1D-Var approach extremely appropriate for deriving TCDRs. As the first step, only temperatures over oceanic surfaces are derived. The 1D-Var system is carefully described. The cloud effects on brightness temperatures at different channels are discussed. Sensitivities of 1D-Var retrieval to water vapor and sea surface temperature variables are investigated. Verifications of the temperature retrieval are made using collocated GPS RO data.

The present study will be extended to an establishment of a temperature TCDR over land from 1998 to 2012 by a direct assimilation of all-channel AMSU-A observations on board NOAA-15, -16, -17, -18, -19, MetOp-A and -B. Influenced of surface emissivity on the AMSU-A observations over land will be taken into consideration to ensure an effective utilization of information contained in those

surface-sensitive AMSU-A channels.

### **Acknowledgement and Disclaimer**

This work was supported by Chinese Ministry of Science and Technology project 2010CB951600 and NOAA satellite calval program. The views expressed in this paper reflect the opinion of the authors and do not represent the US government.

## Reference

- Boukabara, S.A, K. Garrett, W. Chen, F. Iturbide-Sanchez, C. Grassotti, C. Kongoli, R. Chen, Q. Liu, B. Yan, **F. Weng**, R. Ferraro, T. Kleespies and H. Meng: 2011, MiRS: An all-weather 1DVAR satellite data assimilation & retrieval System, IEEE Trans. Geoscience and Remote Sensing, (in press)
- Christy, J. R., R.W. Spencer, and E. S. Lobl, 1998: Analysis of the merging procedure for the MSU daily temperature time series. *J. Climate*, **11**, 2016-2041.
- Christy, J. R.; Norris, W. B.; Spencer, R. W.; Hnilo, J. J., 2007: Tropospheric temperature change since 1979 from tropical radiosonde and satellite measurements, *J. Geophys. Res.*, **112**: D06102. doi:10.1029/2005JD006881.
- Fu, Q., Johnson, C. M., 2005: Satellite-Derived Vertical Dependence Of Tropical Tropospheric Temperature Trends. *Geophys. Research Letters*, **32** (10): L10703.
- Fu, Q. *et al.*, 2004: Contribution of stratospheric cooling to satellite-inferred tropospheric temperature trends. *Nature* **429** (6987): 55–58.
- Liu, Q. and F. Weng, 2005: One-dimensional variation retrieval algorithm for temperature, water vapor and cloud profiles from Advanced Microwave Sounding Unit (AMSU). *IEEE Trans. Geosci. & Remote Sensing*, **43**, 1078-1095.
- Liu, Q. and F. Weng, 2009. Recent stratospheric temperature observed from satellite measurements, *SOLA* **5**: 53–56.
- Hajj, G., C. O. Ao, B. A. Iijima, D. Kuang, E. R. Kursinski, A. J. Mannucci, T. K. Meehan, L. J. Romans, M. de la Torre Juarez, T. P. Yunck, 2004: CHAMP and

- SAC-C atmospheric occultation results and inter-comparisons, *J. Geophys. Res.*, **109**, D06109, doi: 10.1029/2003JD003909.
- Mears, C. A. and F. J. Wentz, 2009: Construction of the Remote Sensing Systems V3.2 Atmospheric Temperature Records From the MSU and AMSU Microwave Sounders. *Journal of Atmospheric and Oceanic Technology*, published online, DOI: 10.1175/2008JTECHA1176.1.
- Mears, C. A.; Wentz, F. J. , 2005: The Effect of Diurnal Correction on Satellite-Derived Lower Tropospheric Temperature. *Science*, **309**: 1548–1551.
- Thorne, P. W., J. R. Lanzante, T. C. Peterson, D. J. Seidel, and K. P. Shine, 2011. Tropospheric temperature trends: history of an ongoing controversy. *Wiley Interdisciplinary Reviews: Climate Change* **2** (2): 66–88.
- Vinnikov, K. Y.; N.C. Grody; A. Robock, R. J. Stouffer, J. D. Philip, and M. D. Goldberg, 2006: Temperature trends at the surface and in the troposphere. *J. Geophys. Res.*, **111**: D03106.. doi:10.1029/2005JD006392.
- Zou, C.; M. Goldberg, Z. Cheng, N. Grody, J. Sullivan, C. Cao, and D. Tarpley, 2006: Recalibration of Microwave Sounding Unit for climate studies using simultaneous nadir overpasses, *J. Geophys. Res.*, **111**: D19114. doi:10.1029/2005JD006798.
- Zou, C.; Gao M, Goldberg MD (2009). "Error structure and atmospheric temperature trends in observations from the microwave sounding unit". *Journal of Climate*, **22** (22): 1661–1681.

Table 1. MSU channel characteristics.

Channel Number	Center Frequency (GHz)	Number of Pass Bands	Band width (MHz)	Center frequency stability (MHz)	NEAT (K)
1	50.30	1	220	10	0.30
2	53.74	2	220	10	0.30
3	54.96	1	220	10	0.30
4	57.95	1	220	0.5	0.30

Table 2. AMSU channel characteristics.

Channel Number	Center Frequency (GHz)	Number of Pass Bands	Band width (MHz)	Center frequency stability (MHz)	NEAT (K)
1	23.80	1	251	10	0.30
2	31.40	1	161	10	0.30
3	50.30	1	161	10	0.40
4	52.80	1	380	5	0.25
5	$53.59 \pm 0.115$	2	168	5	0.25
6	54.40	1	380	5	0.25
7	54.94	1	380	10	0.25
'8	55.50	1	310	0.5	0.25
9	$57.29 = f_0$	1	310	0.5	0.25
10	$f_0 \pm 0.217$	2	76	0.5	0.40
11	$f_0 \pm 0.322 \pm 0.048$	4	34	0.5	0.40
12	$f_0 \pm 0.322 \pm 0.022$	4	15	0.5	0.60
13	$f_0 \pm 0.322 \pm 0.010$	4	8	0.5	0.80
14	$f_0 \pm 0.322 \pm 0.004$	4	3	0.5	1.20
15	89.00	1	2000	50	0.50

**Table 3.** The slope and intercept of a linear fit between MSU channels 1-4 from NOAA-14 and AMSU-A channels 3, 5, 7 and 9 NOAA-15 using SNOs in 2002.

MSU and AMSUA channel	MSU Ch1/ AMSU-A Ch3	MSU Ch2/ AMSU-A Ch5	MSU Ch3/ AMSU-A Ch7	MSU Ch4/ AMSU-A Ch9
Slope	0.976	1.006	1.016	0.964
Intercept	5.358	-0.675	-4.029	7.481
Standard Deviation	0.009	0.019	0.023	0.014

**Table 4.** Same as Table 3 except for CRTM-simulated brightness temperatures using NCEP GFS 6-h forecasts as inputs.

MSU and AMSUA channel	1 and 3	2 and 5	3 and 7	4 and 9
Slope	0.999	1.01	1.003	0.998
Intercept	-0.007	0.008	-0.002	0.008

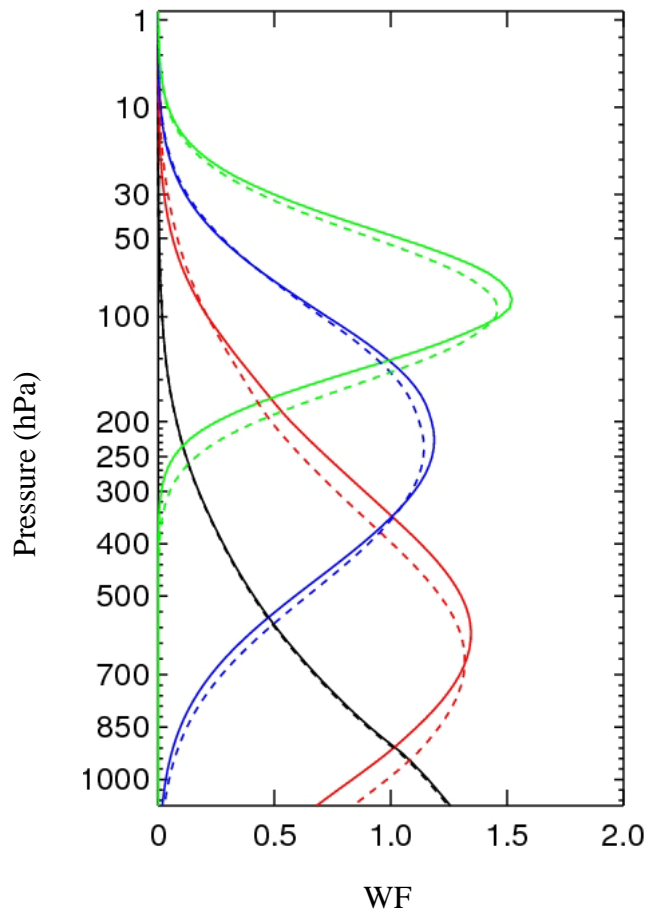


Fig. 1: Weighting functions of MSU channels 1-4 (solid) and AMSU-A channels 3, 5, 7, and 9 (dash) for the US standard atmosphere.

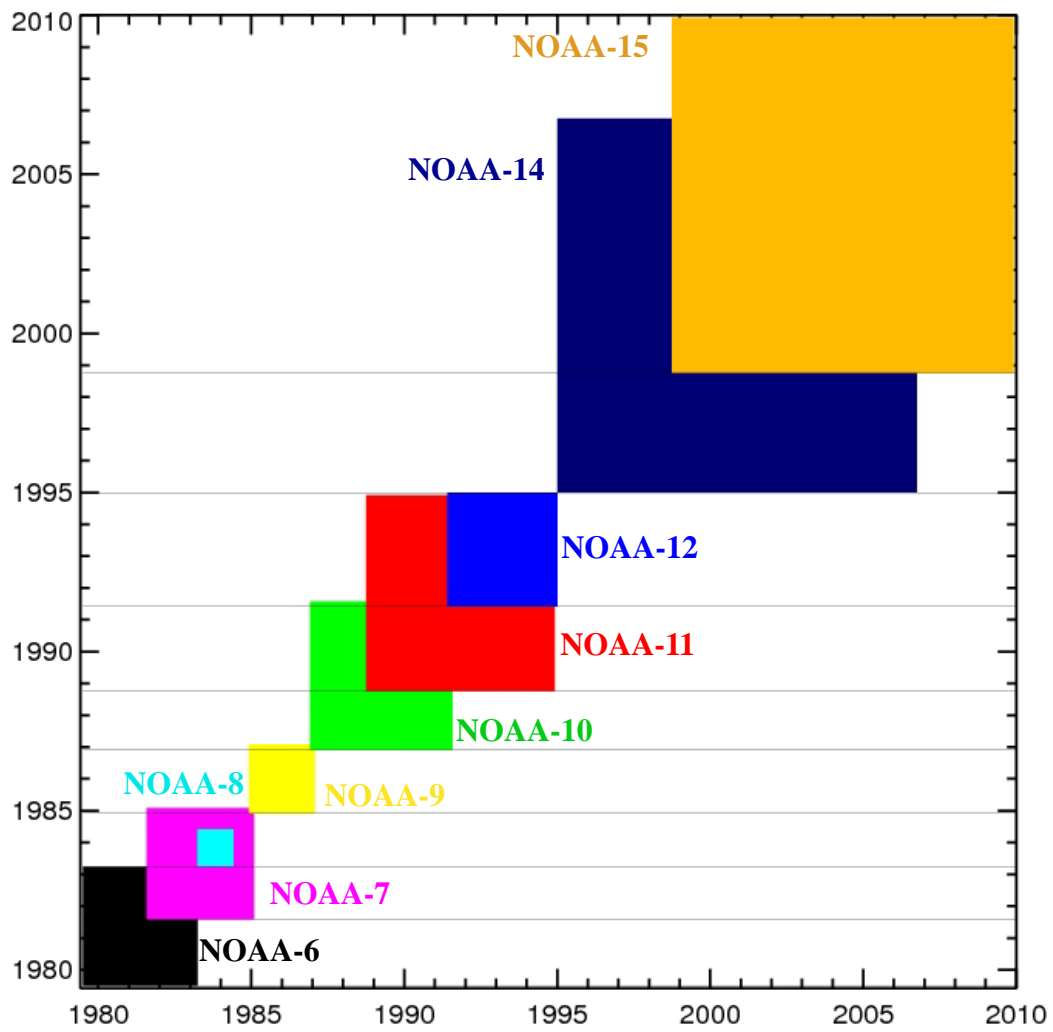


Figure 2: MSU data period on board NOAA's earlier eight polar-orbiting satellites (from NOAA-6 to NOAA-14) and AMSU-A data period on NOAA-15.

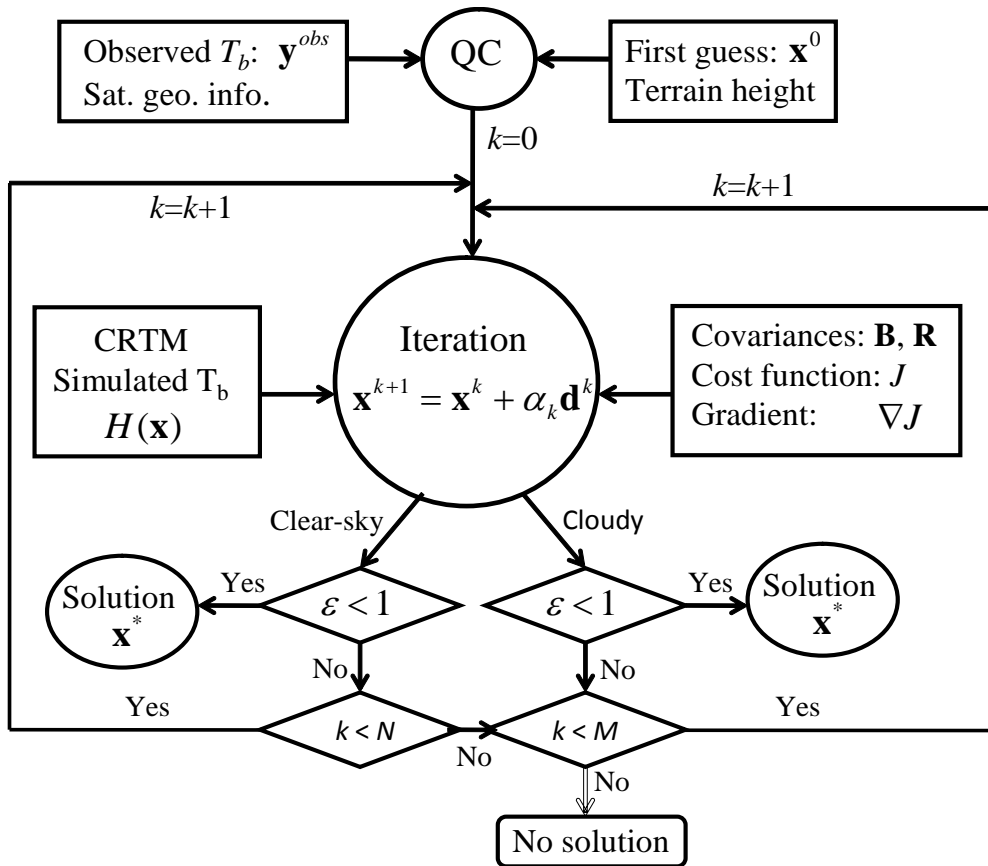


Fig. 3: Schematic illustration of the MSU/AMSU-A temperature retrieval using a 1D-Var approach.

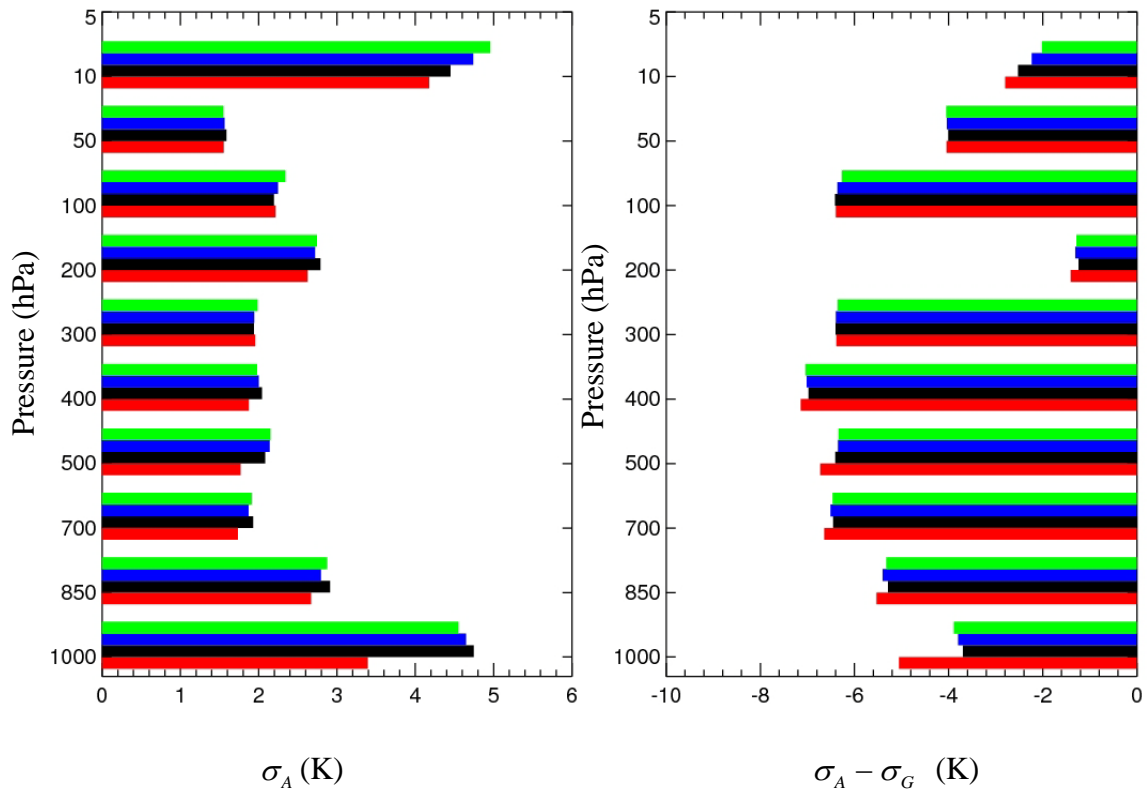


Fig. 4: Global root-mean-square error ( $\sigma_A$ , left panel) and the difference of rmse between the analysis and the first guess  $\sigma_A - \sigma_G$  of temperature retrievals derived from four 1D-Var twin experiments: EXP1 (red), EXP2 (black), EXP3 (blue), and EXP4 (green) at 0000 UTC August 23, 2011.

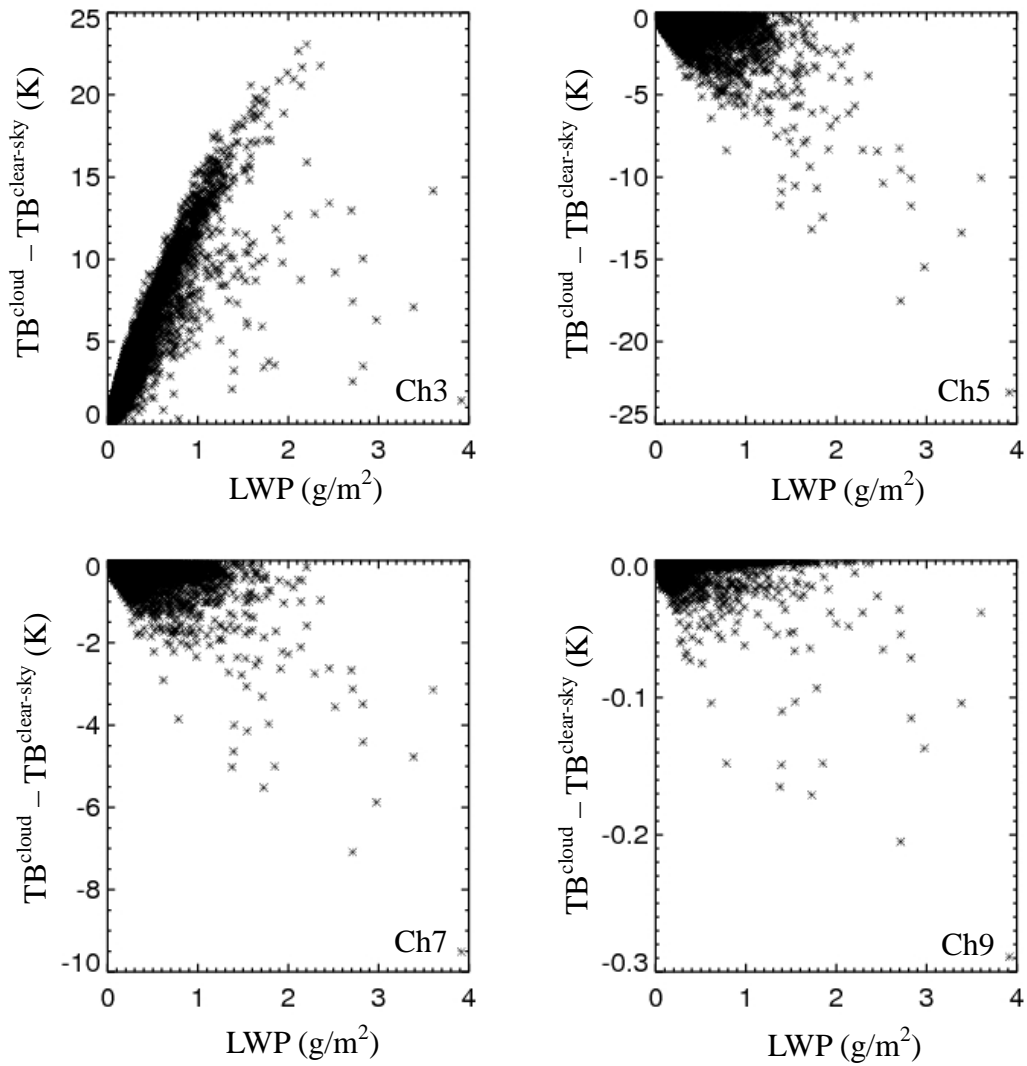


Fig 5: Scatter plots of LWP dependence of model-simulated brightness temperature differences with ( $T_b^{cloud}$ ) and without ( $T_b^{clear-sky}$ ) considering cloud effects in CRTM for all cloudy profiles over ocean on August 25, 2011.

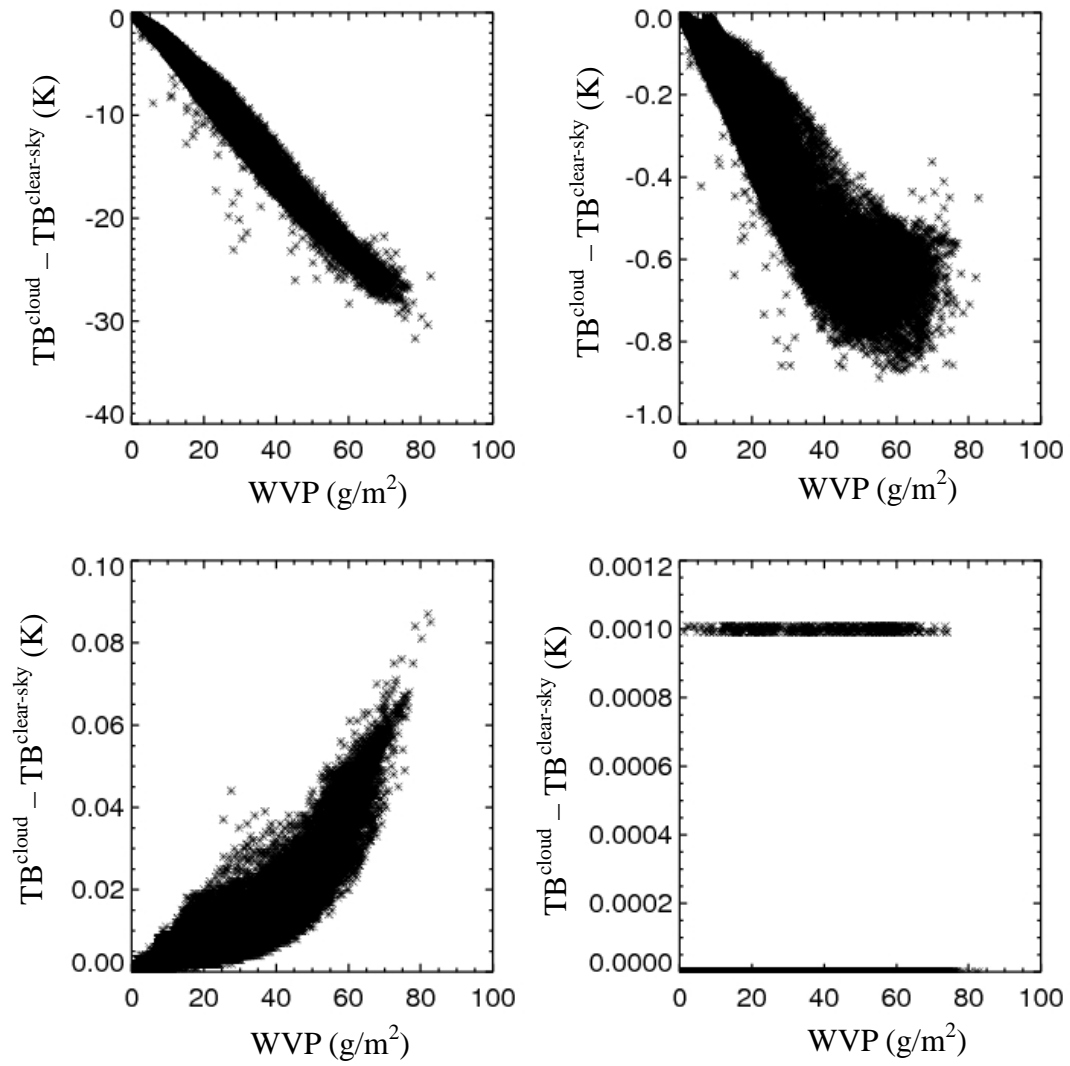


Fig. 6: Same as Fig. 5 except for the variations of  $T_b^{cloud} - T_b^{clear-sky}$  as a function of WVP.

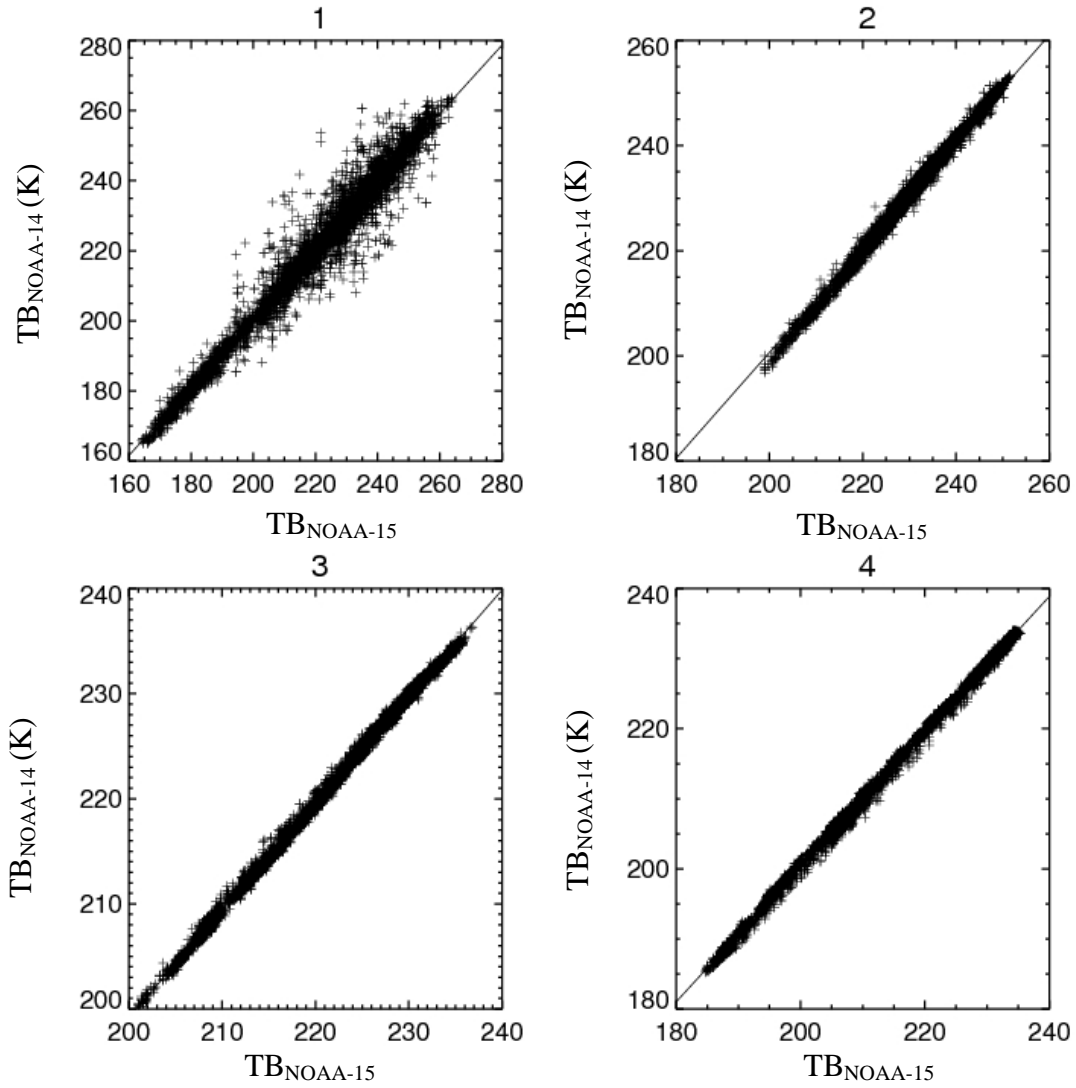


Fig. 7: Scatter plots of the brightness temperature from NOAA-14 MSU channels and the collocated NOAA-15 AMSU-A subset channels for SNO data in 2002. The total number of data count is 5166. Collocation criteria are set as follows: spatial separation  $< 100$  km, and temporal separation  $< 100$  s.

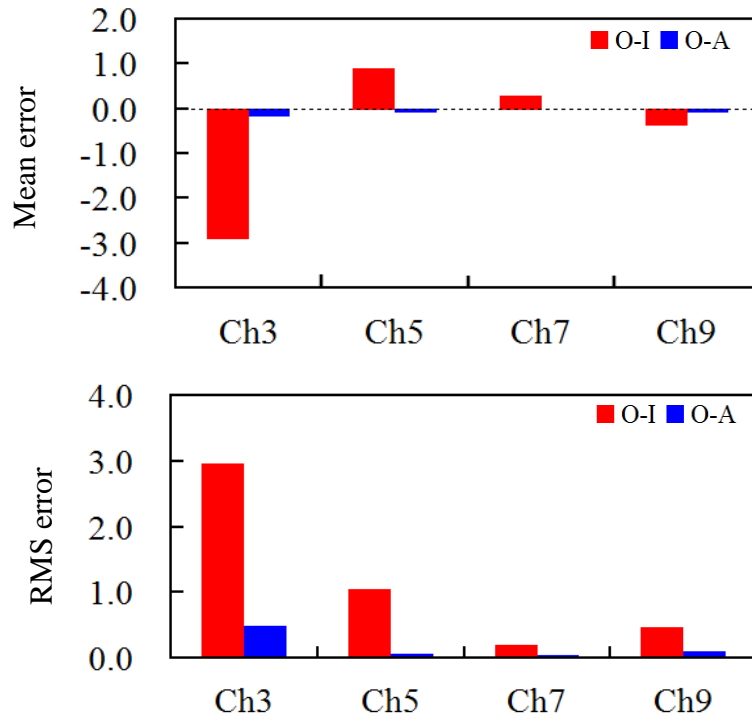


Fig. 8: (a) Mean and (b) RMS differences of brightness temperatures between observations and model simulations from initial guess (O-I, unit: 10K) and 1D-Var analysis (O-A, unit: K) on August 28, 2011.

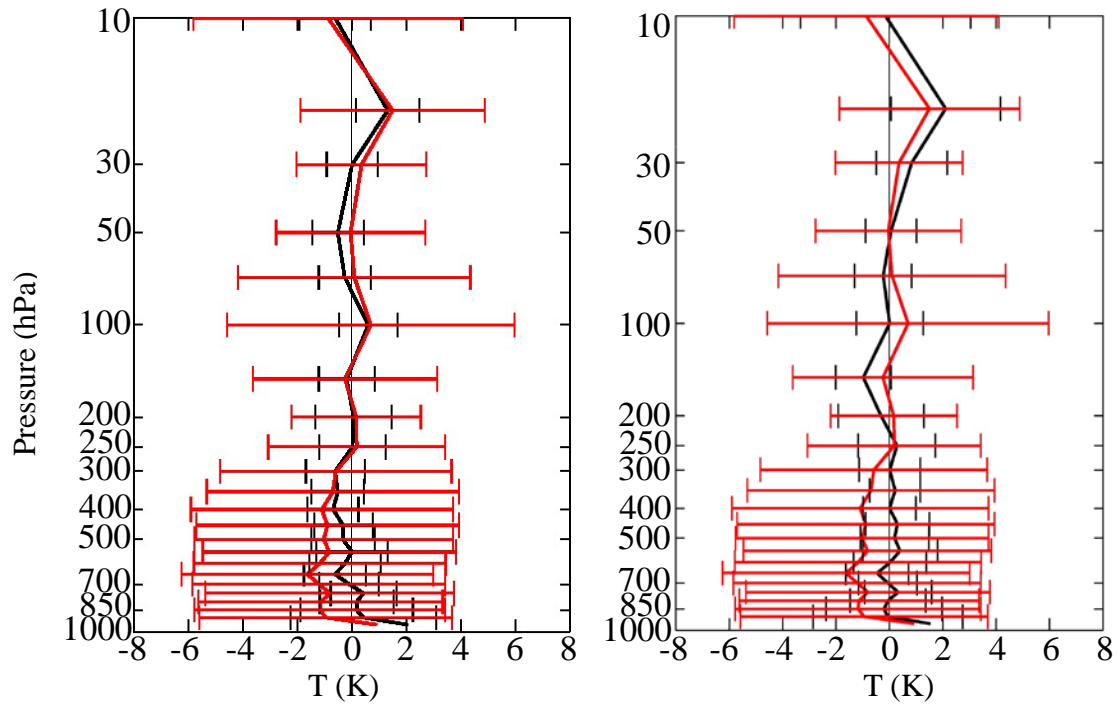


Fig. 9: Mean error (solid) and RMS errors (horizontal bar) of atmospheric temperature profiles from the initial guess (red) and the 1D-Var retrievals (black) verified with COSMIC GPS RO data during June 1-10 in 2008-2011. Collocation criteria in time and space are set to be one hour and 50 km, respectively. (a) Only AMSU-A channels 3, 5, 7 and 9 are assimilated. (b) All AMSU-A channels are assimilated.

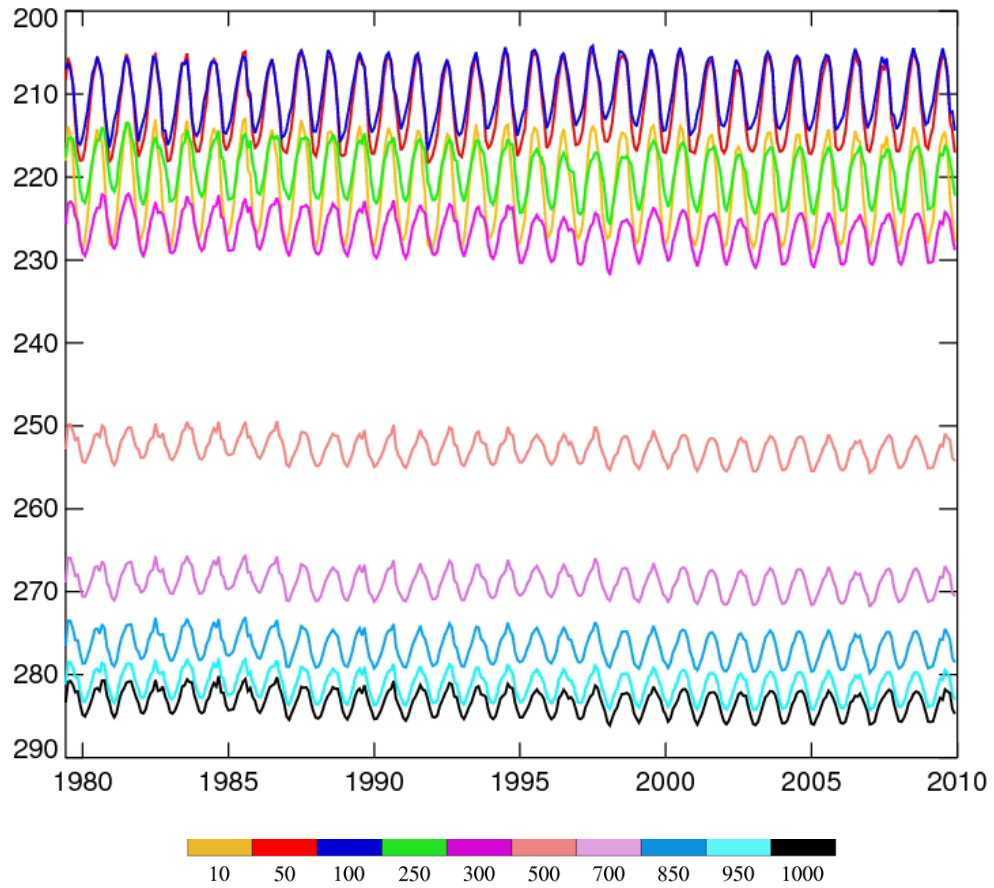


Fig. 10: Monthly and global mean atmospheric temperatures at ten pressure levels retrieved from MSU/AMSU-A brightness temperatures during the 30-year periods from June 1979 to December 2009.

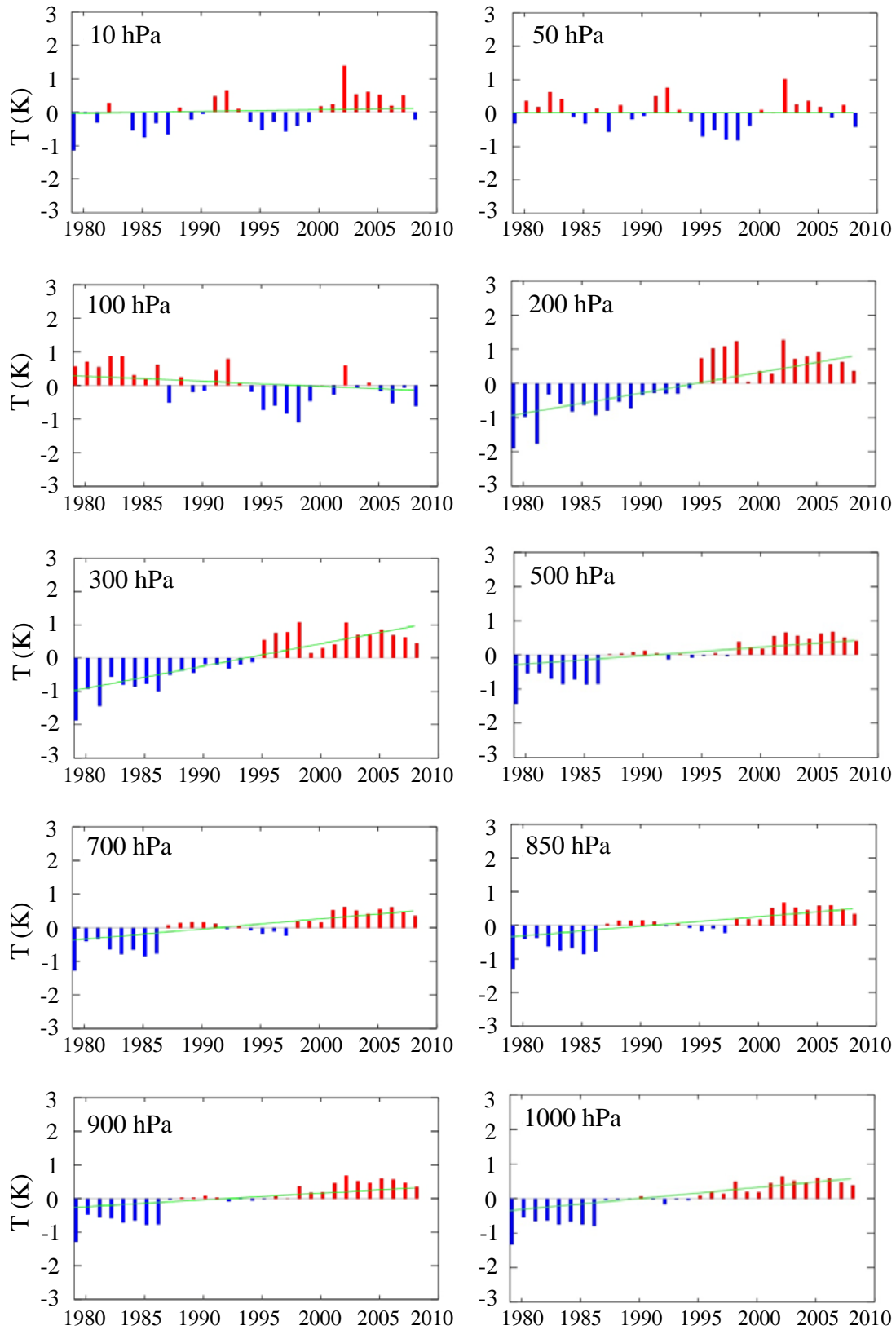


Fig. 11: Annual mean temperature anomaly (bars) at ten pressure levels and the linear trend (green line).

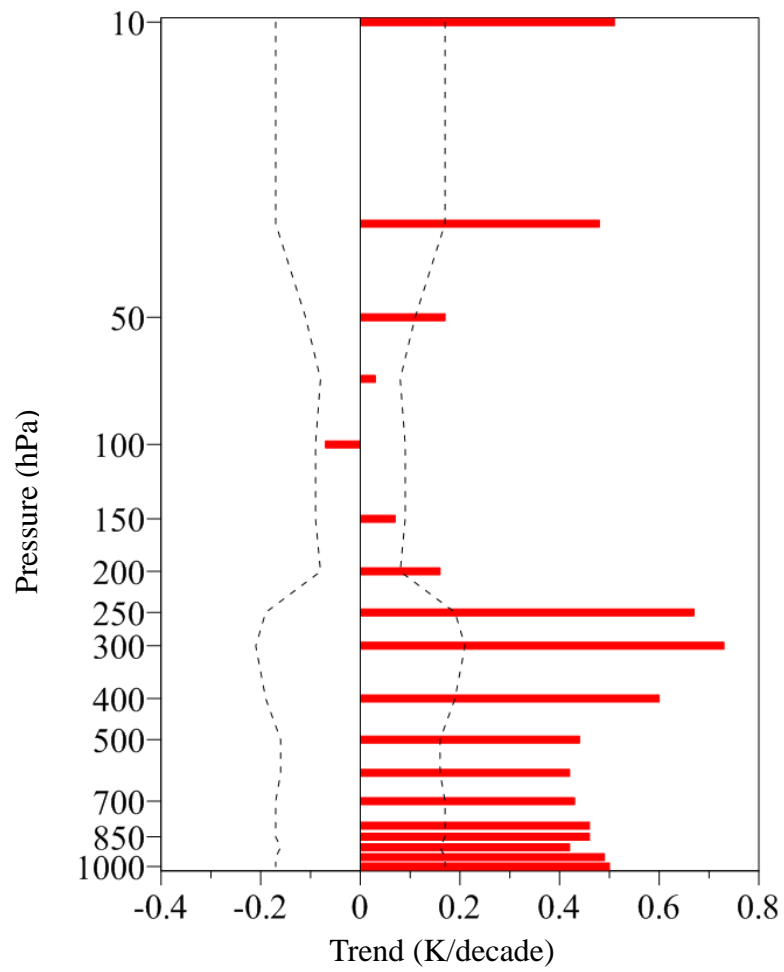


Fig. 12: Global mean temperature trend (red bar) and the uncertainty (dashed) calculated from the temperature retrieval from 1980-2009.